Radio-frequency capacitively coupled plasma parameters evolution as a function of magnetic field strength

Paul Hiret, Artem Dmitriev, E Faudot, Jérôme Moritz, Stéphane Heuraux, F. Brochard, Roland Steiner, Laurent Marot, Alessandro Geraldini, Ivo Furno, et al.

Radio-frequency capacitively coupled plasma parameters evolution as a function of magnetic field strength

Paul Hiret[a], Artem Dmitriev[a], Éric Faudot[b], Jérôme Moritz[b], Stéphane Heuraux[b], Frédéric Brochard[b], Roland Steiner[a], Laurent Marot[a], Alessandro Geraldini[c], Ivo Furno[c], Ernst Meyer[a]

[a] *Department of Physics, University of Basel, Klingelbergstrasse 82, Basel, 4056, , Switzerland*
[b] *Institut Jean Lamour, Université de Lorraine, 2 allée André Guinier, BP 50840, Nancy, 54011, , France*
[c] *Swiss Plasma Center, Ecole Polytechnique Fédérale de Lausanne, route Cantonale, Écublens, 1015, , Switzerland*

Abstract

The use of magnetic fields in low-temperature plasma physics is promising in numerous applications. The magnetic field acts on the kinetic of the plasma charged particles, drastically modifying the ion and electron trajectories in the plasma. The influence of the magnetic field strength on plasma parameters, like the plasma and the electrode potentials, was measured for different gases and pressures, evidencing a strong variation before saturating for high magnetic fields. The saturation is connected to the variation of the ions and electrons collection area. It occurred when the magnetic field influence overcame the collisional effect, *i.e.* when the Larmor radius of ions became smaller than the ion mean free path. The electrostatic probe's floating potential saturation was a marker of ion magnetisation. Varying the pressure enabled collision cross-section calculation for magnetised discharges, leading to values consistent with the literature. Finally, the probe developed in this contribution allows almost independent measurement of perpendicular and parallel flux.

Keywords: Low-temperature plasma, magnetic field, floating potential, electrostatic probe, Langmuir probe

Email address: paul.hiret@unibas.ch (Paul Hiret)

1. Introduction

Magnetic fields in low-temperature plasma physics are widely used. For example, they have promising results in satellite propulsion through Hall effect thruster [1, 2, 3]. Magnetic fields are also used in various applications for controlling capacitively coupled plasmas (CCP) and improving the performance of etching processes in the semiconductor industry [4, 5, 6, 7]. Moreover, in fusion devices, RF discharges are also foreseen for cleaning the first mirrors in optical diagnostics [8, 9, 10].

In a magnetic field B, the charged particle tends to move along the magnetic field lines while rotating around them. In these conditions, the transport of particles perpendicular to the magnetic field is limited and occurs mainly with collisions while the flux along the magnetic field lines remains unchanged [11]. Ions and electrons rotate around the field lines at the cyclotron frequency $\omega_{cx} = q_x B/m_x$ where q_x is the charge, and m_x is the mass of the particle x. The Larmor radius is the radius of the gyromotion that the particle traces around the magnetic field lines. It is given by: $r_{Lx} = v_{\perp,x}/\omega_{cx}$ where $v_{\perp,x}$ is the velocity component of the particle perpendicular to the magnetic field direction. These quantities strongly influence the effect of the magnetic field on the discharge behaviour [12]. In particular, for the case where the collision frequency ν_x is much higher than ω_{cx} (i.e. $\nu_x \gg \omega_{cx}$), the particles will encounter collisions without completing a rotation around the field lines, allowing them to move in the perpendicular direction: the particles are considered not magnetised. Reversely, if charged particles complete several rotations before encountering any collisions (i.e. $\nu_x \ll \omega_{cx}$), the perpendicular mobility will strongly decrease: the particles are considered magnetised. Overall, the degree of magnetisation of the plasma charged species, which determines if the impact of the magnetic field is stronger than the one from collisions, is a vital discharge property to know as soon as the magnetic field strongly impacts the discharge kinetic [12].

This peculiar behaviour of particles in magnetised plasmas complicates the study of their parameters, particularly when using electrostatic probes. Indeed, the variation of the particle kinetics alters the current collection by Langmuir or planar probes used to estimate the discharge properties (potential, temperature, densities,...), leading to a more challenging interpretation of the IV curves in a magnetic field [13]. Stanojevic*et al.* demonstrated that even in relatively weak magnetic fields (around 10^{-2} T), such as those employed in some plasma discharges for materials processing, the distortion of

probe characteristics near the plasma potential due to magnetic field effects can significantly complicate the accurate determination of the plasma potential. This distortion leads to considerable uncertainty, making it challenging to precisely ascertain the electron energy distribution from the measured characteristics [13]. Furthermore, the magnetic field acts on the general current-voltage characteristic curve shape, exhibiting a bumped characteristic between the exponential transition and the electron saturation current regions [14, 15]. The height of the bumps is influenced by the probe inclination to the magnetic field direction, the magnetic field strength, collisional processes, and RF power [15]. Despite various methods to analyse it, the classical approach of determining plasma potential where dI/dV is maximum remains the most reliable, even though some suggest it coincides with the anomaly [14]. The bumped characteristic, which results from density depletion when probe potential exceeds plasma potential, is diminished by increased gas pressure, which enhances perpendicular diffusion, leading to the disappearance of the irregularities [15].

Measurements of plasma density in the plasma column of CCP exhibited increased density in the core of the plasma beam when the magnetic field was increased from 0 to 0.01 mT. In contrast, the density surrounding the column remained similar to the one measured without a magnetic field [16]. Yadav*et al.* observed similar radial variations of the temperature and density in helicon discharges [17]. They showed that, in magnetic fields, the electron pressure was higher at the edge of the column than at the centre. Moreover, the electron pressure values saturated when the ion Larmor radius became less than half of the discharge chamber radius, *i.e.* when ions were magnetised. Similar saturations of plasma parameters were observed on measured floating potential by Filleul*et al.* when the Larmor radius became shorter than the chamber radius [18].

Despite a few experimental characterisations of plasma bulk in magnetic fields, the effect of magnetisation on low-temperature plasma bulk parameters has not been widely measured in large magnetic fields ($> 0.3\,T$). Understanding the behaviours of charged particles in such discharges is necessary to improve plasma etching that operates in high magnetic fields, such as the first mirror cleaning in next-generation fusion devices. In this contribution, we conducted an experimental characterisation of the plasma bulk using a planar and a radial probe in a varying magnetic field up to 3 T.

2. Experiments

2.1. Basel University Magnetised Plasma (BUMP)

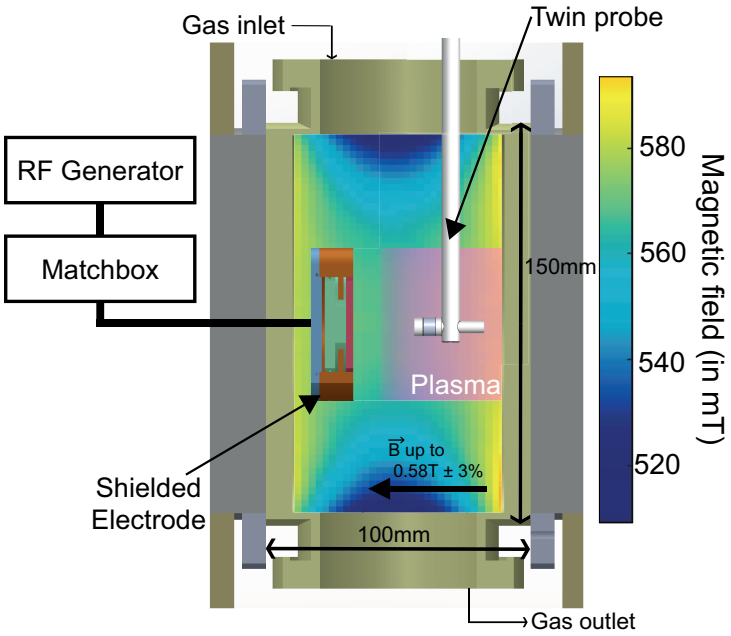

Figure 1: Experimental setup: BUMP.

Plasma discharges were carried out in the Basel University Magnetised Plasma (BUMP). The facility consists of a 100 mm long and 150 mm wide chamber installed between the two water-cooled coils of an electromagnet Bruker B-E 15 powered by a Bruker B-MN90 power unit. The background pressure in the vessel was around 10^{-4} Pa. By varying the current in the coils, the magnetic field inside the chamber can be increased up to 0.58 T. The field homogeneity at this magnitude is presented in figure 1. The magnetic field varies by 10% in the chamber but only by 3% around the electrode. A 50 mm-diameter circular shielded copper electrode was set up inside the vacuum chamber. The electrode was centred in the vacuum chamber but shifted closer to the wall in the magnetic field direction to fit the electrostatic probe. The surface of the electrode was also coated with tungsten to reduce erosion and, therefore, deposition on the probe. Most of the CCP discharges were driven by a 13.56 MHz RF generator (Huttinger Elektronik GmbH and Co KG, model PFG 300 RF) coupled with a matchbox (Huttinger Elektronik

GmbH and Co KG, model PFM 1500A). Some of the discharges were driven with a 60 MHz generator (Comet Cito 600W with Agilo matchbox). The matchboxes are equipped with a voltage probe allowing for measuring the self-bias potential V_{DC}. The error on bias voltage measurements was typically in the range of 5 V. The measurements of the bulk plasma parameters were carried out utilising the twin probe, described in the following section.

2.2. Twin probe

As mentioned in the introduction, when the magnetic field increases, the charged particle rotates around the magnetic field lines, leading to a reduced perpendicular flux $\Gamma_\perp$ while the parallel flux $\Gamma_\parallel$ remains unchanged. For experimental quantification of the flux changes, the twin probe was designed and manufactured, allowing for the measurement of these variations.

The twin probe is an electrostatic probe made of two electrodes: a planar electrode and a radial electrode (Figure 2). The planar electrode consists of a 5 mm diameter titanium disk perpendicular to the magnetic field. The radial probe is made of a 5 mm diameter and 4 mm long titanium cylinder. Only the outer surface of the radial electrode was in contact with the plasma. The rest of the titanium was covered with ceramic, as shown in Figures 1 and 2. The electrodes were fixed on a ceramic holder. Both electrodes were independently connected to an RF-compensated ESPion Langmuir probe from Hiden Analytical Ltd. While one electrode was biased, the second one was floating (i.e. at the floating potential V_f). The planar probe, which is perpendicular to the magnetic field, is mainly collecting the parallel flux (Figure 2(a)). However, a small part of the perpendicular flux is also collected as a sheath develops around the probe while biasing it. Reversely, in the case of the radial electrode, the surface is parallel to the B field, leading to the collection of the perpendicular flux and a tiny part of the parallel flux.

The twin probe was installed in the chamber in front of the electrode. The planar probe faced the discharge electrode and was slightly shifted toward the wall to ensure that the probe was not in the electrode sheath.

To benchmark the developed twin probe, an ESPIon Langmuir probe with a cylindrical tip 10 mm long and 0.075 mm radius was mounted in non-magnetised Ar plasma at various pressures. The plasma parameters measured on both electrodes of the twin probe differed by a maximum of 10% from those measured with a commercial Langmuir probe, which is in the typical plasma parameter measurement error of a Langmuir probe in non-magnetised plasmas($\pm$20%) [19]. The complexity of the current-voltage

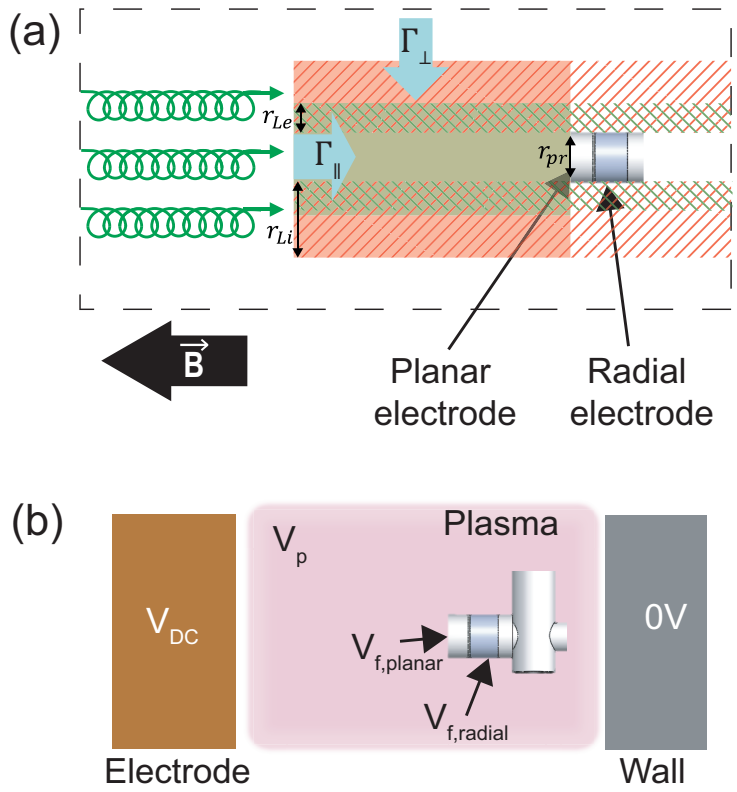

Figure 2: Schematic of the working principle of Twin Probe (a) and of the different measurable potential (b). In the limit of collisionless plasma, the ions are collected from the red flux tube and the electrons from the green one. Particles in the hatched tube are collected on the radial probe.

probe characteristics analysis in a magnetic field can be responsible for a more significant error in magnetised discharges.

2.3. I-V curve analysis

2.3.1. Without magnetic field

The current-voltage curve collected by the probe is related to plasma properties, particularly the floating potential V_f, the plasma potential V_p, the plasma density n_0 and the electron temperature T_e. The floating potential corresponds to the probe's potential for which zero net current is collected. It is also the potential at which the probe will float naturally if no bias is applied. In non-magnetised capacitively coupled discharges, the

electron temperature is related to the slope of the logarithm of the electron current collected by the planar probe below the plasma potential. At a more positive bias than the floating potential, the electron current increases until there is no retardation of electrons. At higher potentials, the exponential retardation current is replaced by the collection of electrons due to the sheath growth around the probe, which exhibits a flatter slope with respect to potential. The transition between these two contrasting regimes of electron collection can be identified as an inflexion in the probe characteristic, which is determined by the derivative peak at V_p. The plasma density can then be determined from the ion saturation current and the electron temperature [11, 20].

2.4. In magnetised plasma

A strong external magnetic field modifies the behaviour of the charged particles in the plasma. These changes drastically alter the fluxes collected by a surface inclined to the magnetic field. The flux along the magnetic field line is unaffected; however, the transport of particles perpendicular to the magnetic field occurs only due to collisions [11], leading to a more challenging interpretation of the IV curves in a magnetic field. In this manuscript, the method developed by Stangeby and then by Stanojevic [21, 13] was used to extract the discharge properties from the probe current-voltage characteristics. For a planar probe introduced in a plasma perpendicularly to the magnetic field B and assuming that the probe's effective ion collection area approximately equals its geometrical area A, the current I_i drawn down from a long flux tube below the floating potential can be written as:

$$I_i = I_i^s \left(1 - \exp\left(\frac{e(V - V_f)}{k_B T_e}\right)\right) \tag{1}$$

with $I_i^s = \alpha \cdot ZeAn_0\sqrt{k_B T_e/m_i}$ the ion saturation current and Z the average ion charge number. In a magnetic field, $\alpha = 0.7$ due to the enhanced density in front of the sheath [21].

The floating potential V_f is determined by the zero net current potential. T_e and I_i^s can then be determined as fitting parameters in a non-linear fit of the equation 1 applied to the portion of the measured characteristic below V_f. After deriving T_e, the plasma density (n_e) can be calculated from I_i^s. Considering the error due to plasma RF fluctuations prevail, the method

described in the previous section remains valid for determining the plasma potential for relatively low magnetic fields [22].

3. Results and Discussions

3.1. Plasma parameters

The self-bias V_{DC} was measured in Ar 13.56 MHz CCP for varying magnetic fields, gases and pressures. Without a magnetic field, as a classical CCP discharge, a negative V_{DC} developed due to the asymmetry between the powered and grounded area. Indeed, the grounded wall-to-powered electrode area ratio is roughly 20, resulting in a few hundred volts of negative self-bias. Increasing the magnetic field led to an exponential increase before reaching an asymptotic plateau (figure 3). In Ar discharges, that saturation occurred around 30 mT at 2 Pa.

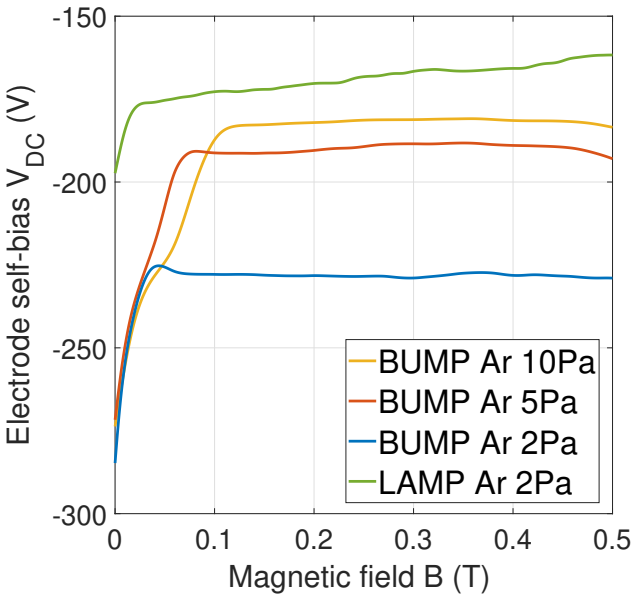

Figure 3: Electrode self-bias variation with the magnetic field for different pressure and vessels in Ar discharges driven at 13.56 MHz (10W).

In addition to the self-bias, plasma density, temperature and potential were measured using the twin probe. Similar to the electrode self-bias, the plasma potential, which is also strongly dependent on the plasma asymmetry [23, 5, 24], increases with B field after several mT, before saturating at a

similar field strength as the self-bias (figure 4). The floating and plasma potential measured by the planar and radial electrodes of the twin probe start to decrease at the first stage of the magnetic field increase up to a few mT. Caldarelli measured similar decreases in the plasma potential for an increasing B field from 7 to 33 mT [25]. For higher magnetic field intensity, V_p and V_f increased until nearly saturating (figure 4, a detailed view focusing on the range of a few mT to 0.2 T is provided in supplementary material figure S1). A similar dependency of the floating potential with the magnetic field was measured at low-pressure (0.13 Pa) in Ar discharges in a magnetic nozzle device by Filleul*et al.*, where the changes in V_f were expected to be driven by the magnetisation of the ions [18]. Indeed, they showed that V_f saturated when the bulk ion Larmor radius r_{Li} gets three times smaller than the shorter plasma length scale (the chamber radius in their case) corresponding to a magnetic field of 50 mT. In Filleul*et al.*, the mean free path was greater than the chamber scale, so the chamber radius was considered instead of λ_i. In this study, the chamber radius (75 mm) is always larger than the ion mean free path, which is a maximum of 16 mm at 0.5 Pa.

The effects of gas pressure and gas type are discussed in the following sections. Finally, hypotheses are proposed to explain the variation of the plasma parameters in terms of plasma confinement and ion magnetisation.

3.2. Collisional effect

The magnetic field at which the self-bias saturated was measured for different pressures in two distinct experimental vessels with different area ratios (BUMP and LAMP [26]) with Ar at 13.56MHz (in blue dots, figure 5). The magnetic field saturation threshold, *i.e.* the magnetic field at which the self-bias saturated, increased with the pressure following the $\lambda_i(p) = r_{Li}(B)$.

The magnetic field at which the floating potential (radial: red square; planar: yellow triangle) and the self-bias (in blue dots) saturated was measured for different pressures p from 0.5 Pa to 10 Pa in Ar discharges (figure 5). In the following, the magnetic field at which the potential saturates is called the saturation magnetic threshold. As for V_{DC}, the saturation magnetic threshold for V_f (radial and planar) increased with the pressure in line with the increase in collisionality. Additionally, several measurements were carried out at 60MHz. The RF frequency did not affect the magnetic threshold of the self-bias and floating potential in Ar discharges, as it mainly affected the overall density of the plasma and not the collisionality (figure 5).

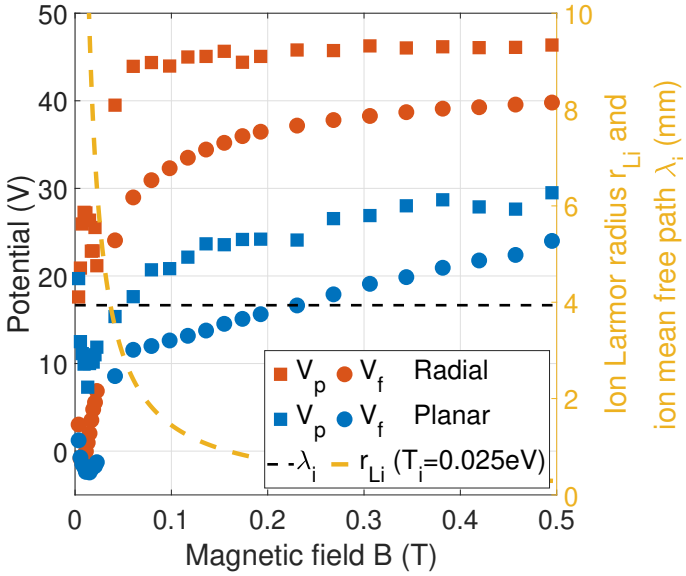

Figure 4: Plasma and floating potential variation as a function of the magnetic field at 2 Pa in Ar discharges driven at 13.56 MHz (10W). The error on potential measurement was ±5 V. The ion Larmor radius r_{Li} and the ion mean free path λ_i are also displayed with their scale shown on the right y axis.

As mentioned in the introduction, theoretically, magnetisation occurs when $r_{Li} < \lambda_i$ [12]. As $r_{Li} = m_i v_\perp / eB$ and $\lambda_i \approx k_B T_g / p\sigma$, where m_i is the mass of ion, T_g the neutral gas temperature and σ the ion-neutral elastic and charge-exchange collision cross-section, it occurs for a magnetic field:

$$B > \frac{m_i v_\perp}{e k_B T_g} \sigma p \approx 2.5 \times 10^{16} \cdot \sqrt{m_{i,u} T_{i,eV}} \cdot \sigma_{eff} p \qquad (2)$$

where $m_{i,u}$ are the ion mass in atomic unit u $T_{i,eV}$ is the ion temperature in eV and σ_{eff} is the effective collision cross section in the plasma. In our conditions, the ions and the neutrals are not subjected to significant heating [27, 28]; $T_{i,eV}$ is then approximated to the room temperature 0.025 eV as the gas temperature. However, in addition to gyromotion, various drifts affect the plasma kinetic and the collision process in a magnetic field. The potential profile in figure 6 displays a difference of potential from the centre of the plasma column (28V at r=0 mm) to the edge of the plasma column (45 V at r=25 mm) at 0.1 T. That difference of potential is responsible for an electric field toward the core of the plasma beam as high as 680 V.m^{-1},

leading to a strong $E \times B$ drift in the azimuthal direction (≈ 4500 m.s^{-1} at 150 mT) as previously reported [29, 26]. Moreover, the measured electron pressure profile (figure S2) indicated the presence of a diamagnetic drift in the same azimuthal direction. Indeed, the pressure gradient is directed toward the column core (figure S2) as the electric field. Khrapak reported that when ions are subjected to drift velocity caused by the external electric field higher than the thermal velocity, the collision cross-section appeared to be reduced by a factor 2 to 3 for Ar [30]. It has also been reported that in the presence of a magnetic field, the collision frequency could be reduced by a factor of 2 due to the reduction of the travelled distance in the perpendicular direction when $r_{Li} \approx \lambda_i$ [31]. Considering the influence of the drift on the effective collision cross-section $\sigma_{eff} = \sigma/2.2$ (for Ar), equation 2 for with σ_{eff} becomes:

$$B > 1.1 \times 10^{16} \cdot \sqrt{m_{i,u} T_{i,eV}} \cdot \sigma p \tag{3}$$

The equation 3 was used to fit the magnetic threshold of floating potential values measured with the planar electrode of the twin probe in Ar (yellow triangle in figure 5), using the cross-section as a coefficient. With Ar, the experimental value of σ was found to be around 1.2×10^{-18} m^2 which is coherent with typical values of cross-sections, including ion-neutral elastic collisions and resonant charge-exchange, which are about 10^{-18} m^2 in the literature [32, 33, 34, 11]. The planar probe and the self-bias measurements exhibited good agreements with the effective collision cross-section of Khrapak [30] and the one measured by Maiorov [33] considering the attenuation factor from Khrapak calculations. Additionally, it is similar to the approximation given by Tsankov *et al.* [12] reduced by Khrapak's factor. The magnetic thresholds were higher than equation 3 using the kinetic theory cross-section (black line on figure 5). Indeed, the kinetic theory considers only the elastic collision. Nevertheless, the number of charge-exchange collisions is in the same order for Ar and contributes significantly to the impact of collision on perpendicular diffusion.

Furthermore, the radial floating potential saturated at a higher B field magnitudes when $r_{Li} \ll \lambda_i$, which is in line with the criterion for magnetisation commonly used [12, 18, 11].

3.3. Gas impact

Additionally, the influence of the gas on the plasma magnetisation and confinement was studied using different gases in BUMP (figure 7). Hydrogen

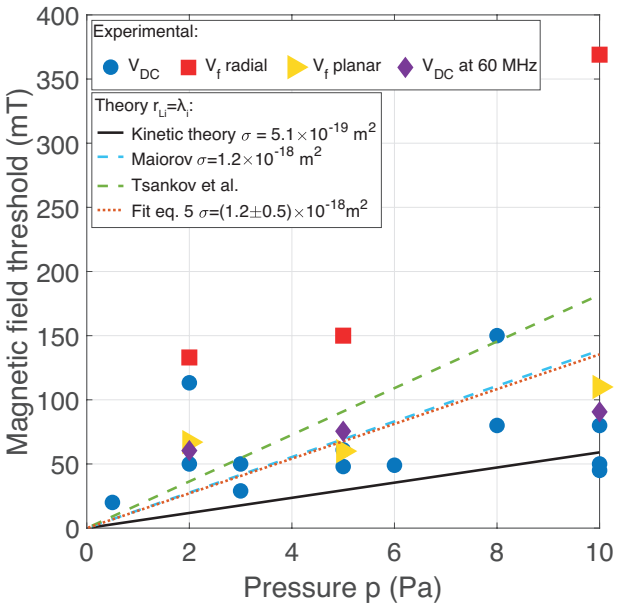

Figure 5: Pressure variation influence on the magnetic threshold for V_{DC} and V_f saturation for Ar. The error was ±20%.

(H_2), deuterium (D_2), helium (He) and neon (Ne) were studied in addition to Ar at 10 Pa and 13.56MHz. Using the equation 3, the values of total collision cross-sections were calculated to be $\sigma_{He} \approx 1 \times 10^{-18}$ m^2 for He and $\sigma_{Ne} \approx 2.5 \times 10^{-19}$ m^2 for Ne, using the self-bias measurements at 10 Pa. The values of σ_{He} were in a similar range to the values reported by Maiorov despite a factor 2 to 2.5 (5.6×10^{-19} m^2 for He and 6.4×10^{-19} m^2 for Ne) [33].

The V_{DC} and V_f magnetisation thresholds were also measured for H_2 and D_2 (figure 7). For all the gases from H_2 to Ar, the measured V_f magnetic threshold with the planar probe was close to the calculated threshold given by Tsankov*et al.* [12] refined considering drift velocities. However, the saturation of the probe floating potential in the plasma column showed a correlation with the $r_{Li} = \lambda_i$ considering the kinetic theory for the calculation of the ion mean free path [35] (figure 7).

Lastly, the radial floating potential magnetic threshold corresponds to $r_{Li} \approx \lambda_i/3$, consistent with the pressure variation measurements described in the previous section.

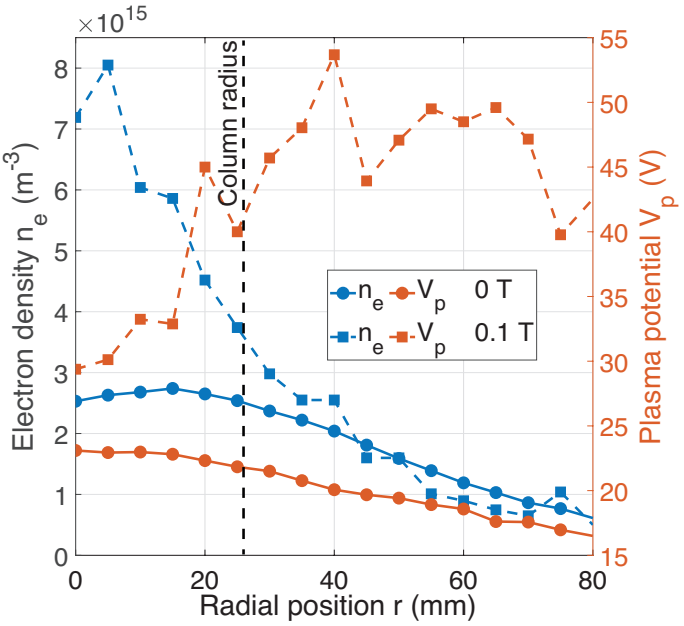

Figure 6: Radial profile of the bulk plasma electron density and plasma potential at 1 Pa in Ar discharges driven at 13.56 MHz (10W). The error was ±20%.

3.4. Plasma confinement

In the previous sections, the saturation of self-bias and floating potential were measured and linked to the magnetisation of the ions through the ion magnetisation criteria. In the following, the relation between self-bias and plasma confinement is discussed. In non-magnetised asymmetric CCP, when the plasma expands in the whole vessel and the grounded wall area is larger than the area of the powered electrode, a self-bias (usually negative) develops on the powered electrode [36, 23, 5, 24]. In the following section, plasma confinement will be referred to as limiting, constraining the plasma expansion. Later, the magnetic field line will play this role, and not the vessel walls, *i.e.*, increasing the magnetic field will decrease plasma volume. The action of confinement will evolve to a steady state plasma volume for a specific field strength. At this magnitude, the wetted plasma area is constant, and the wall-to-electrode area ratio no longer varies.

As mentioned in the previous sections, the self-bias V_{DC} was measured in Ar 13.56 MHz CCP for varying magnetic fields, gases and pressures. It was found to increase exponentially with a rising magnetic field before reaching a

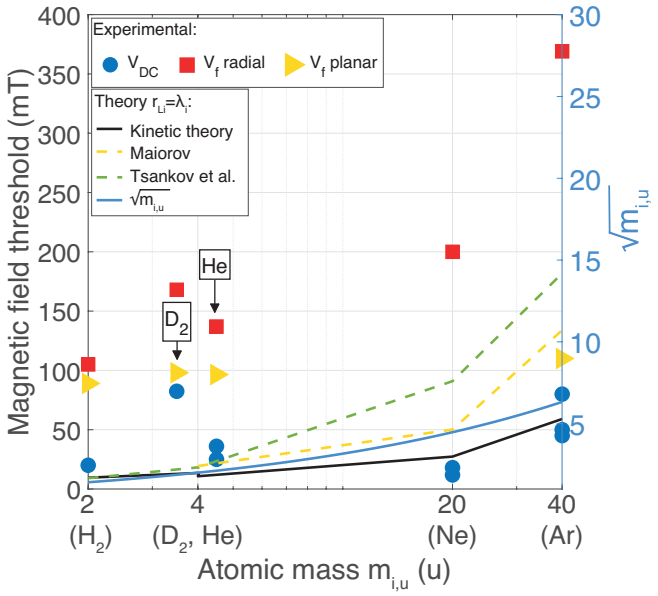

Figure 7: Magnetic threshold for V_{DC} and V_f saturation with different gases. For better visualisation, D_2 and He were arbitrarily split around the mass 4.

plateau corresponding to the magnetic confinement of the CCP (figure 3). As a classical CCP discharge, without a magnetic field, a negative V_{DC} developed due to the asymmetry between the powered and grounded area. Indeed, the grounded wall-to-powered electrode area ratio is roughly 20, leading to a few hundred volts of negative self-bias. When the magnetic field increases, the charged particles rotate around the field lines, confining most of the plasma in a column if we neglect collisions. The radius of this column r_c equals the sum of the electrode r_p and the ion Larmor radii (*i.e.* $r_c = r_p + r_{Li}$). The column size and, therefore, the wall surface in contact with the plasma column diminish with an increasing magnetic field, such as the Larmor radius. The grounded chamber is a cylinder, so the wetted area A_w equals the total area of the vessel when $r_{Li} + r_p \geq R$ where R is the chamber radius (figure 8). Indeed, the large Larmor radius allowed the particle to reach the lateral surface of the chamber. However, when $r_{Li} + r_p < R$, the ions in the column cannot reach the lateral surface of the wall without collision, the wetted surface is then $A_w = \pi(r_{Li} + r_p)^2$. In BUMP, the relation $r_{Li} + r_p < R$ is verified for B field magnitude superior to 3 mT for Ar at room temperature.

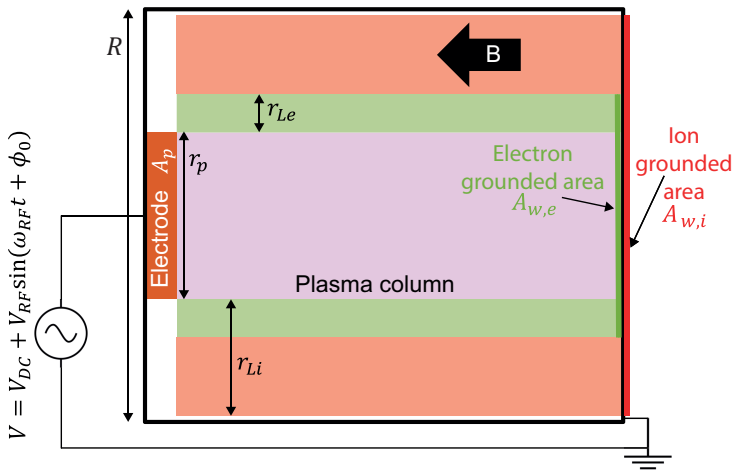

Figure 8: Schematic of surface collection of ions and electrons.

To investigate the variation in plasma volume confinement, we measured the radial profile of electron density at 1 Pa, showing a threefold increase in n_e at the centre of the plasma column as the magnetic field increased from 0 to 0.1 T (figure 6). A similar density increase was reported for a rise in the magnetic field from 15 to 80 mT [37]. Nevertheless, the measured density cross-section profile exhibited that if some of the particles were confined in the cylindrical plasma column, there was still a residual plasma around it, in contact with the rest of the chamber and participating in the geometrical asymmetry of the discharge, as shown on the density cross-section profile measurement in figure 6. Even when the area wetted by the plasma column on the ground wall decreased, the area that was no longer covered by the column became wetted by the low-density plasma. That led to an increase in the residual plasma's contact area, similar to the reduction of the column. Soni*et al.* observed that the variation with a magnetic field of the column-wetted area on the ground wall when the magnetic field was strong enough was the leading cause of variation of self-bias [38]. Considering that only the plasma column wetting the powered electrode influenced the variation of the self-bias, the area ratio $A_w/A_p = (1 + r_{Li}/r_p)^2$ then saturated (*i.e.* $A_w/A_p < 1.05$) for B=23 mT in BUMP and LAMP (r_p =50 mm).

However, experimentally, at 2 Pa, the self-bias V_{DC} (and so of the area ratio) saturated at a B field of $\approx$ 40 mT, which was higher than the 23 mT calculated considering only the magnetic field impact (figure 3). That differ-

ence between the theoretical and experimental values appears to be caused by the collisional expansion of the plasma column. Indeed, collisions allow the ions to travel perpendicularly to the field line further than their Larmor radius. It was also shown that when the pressure p increased, the self-bias saturated at higher magnitudes (figure 3). Indeed, higher pressure increased the collisionality of the plasma. When the ion mean free path, which depends on the pressure and the gas temperature T_g (corresponding to the room temperature), is smaller than the ion Larmor radius ($\lambda_i = k_B T_g / p\sigma > r_{Li}$), most of the ions do not complete a full rotation around the magnetic field lines, which leads to a higher particle diffusion in the perpendicular direction to the magnetic field and so to lower confinement efficiency. This lower confinement is responsible for the shift to a higher B field of the saturation of the self-bias due to the collisional effect. The influence of collisionality is detailed in section 3.2 of this manuscript.

From 0 to several mT (2 mT at 2 Pa), the electrons get magnetised and rotate with a Larmor radius much smaller than the electron-neutral collision mean free path and the chamber radius, while the ions are not magnetised. The electrons are then more easily confined in a column and collected on the electrode and on the plasma column opposite disc. At the same time, the ions are collected on all the surfaces of the chamber and electrode. However, due to their extremely small Larmor radius r_{Le}, the electrons are hardly collected on the lateral surface of the vessel, even at a B field of 10 mT. As the collection surface of electrons decreases while the ions collection area does not, the plasma potential in the column, which is responsible for the electric field in the grounded wall sheath (in contact with the column), has to reduce, to diminish the electron retardation and so increase the electron flux on electron collection surfaces of the wall ($A_{w,e}$ and A_p on figure 8). Increasing the magnetic field further reduces the wall effective area for ions, which cannot reach the lateral surface anymore without any collision; the plasma potential increases then to balance electron and ion flux to the wetted surfaces. The plasma potential saturates when the ion and electron collection areas are both saturating. That saturation indicates that the diffusion parallel to the magnetic field is larger than the perpendicular diffusion; in other terms, the influence of the magnetic field is in the order of the collisional effect. At 2 Pa with Ar, this saturation is reached around 60 mT (figure 4). That corresponds to the magnetic field at which $\lambda_i = r_{Li}$ (figure 4).

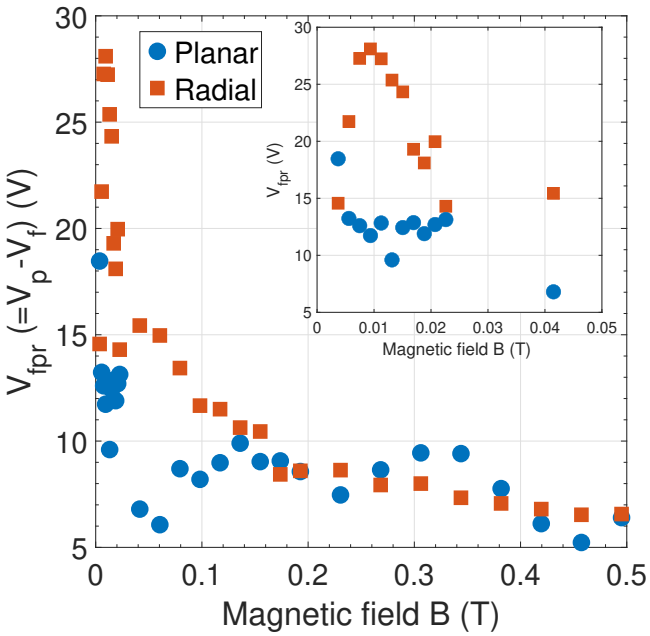

Figure 9: $V_{fpr} = V_p - V_f$ in the plasma bulk as a function of the magnetic field in 2 Pa Ar discharges driven at 13.56 MHz (10W). The error on V_{fpr} was ±5 V.

3.5. Plasma magnetisation

In the previous sections, the saturation of self-bias and floating potential were measured and linked to the magnetisation of the ions. The following discusses the relationship between floating potential and ion magnetisation. As mentioned in the introduction, the charged particles are magnetised when the influence of the magnetic field dominates the impact of collisions, *i.e.* when $r_L \ll \lambda$ [12]. The magnetisation of the plasma is considered reached when all the ions and electrons are magnetised. In this condition, the perpendicular diffusion saturates, mainly caused by collisions.

Due to its design, the radial electrode of the twin probe mainly collected the perpendicular flux, and the floating potential is then linked to the perpendicular diffusion. Reversely, the planar electrode collected mainly the parallel flux. In figure 9, the floating potential relative to the plasma potential, $V_{fpr} = (V_p - V_f)$, is proportional to the electric field in the vicinity of the probe responsible for balancing the ion and electron current. One can see in figure 9 that $V_{fpr,planar} \approx V_{fpr,radial}$ at 0 T, however increasing the

magnetic field led to $V_{fpr,radial} > V_{fpr,planar}$ at 0.05 T. The potential difference between the plasma and the probe increases to raise the ion flux to the probe when electrons are magnetised. Indeed, due to the rotation around the field lines, the electrons from the annular flux tube around the probe are easily collected, while the ions, not magnetised, are collected mainly due to the perpendicular diffusion caused by collision (figure 10). With further increase of the magnetic field, more ions are completing rotation around the field lines, encountering a minimal number of collisions, the ion flux to the probe increases, and $V_{fpr} = V_p - V_f$ decreases to balance the ion and electron currents. When the ions are completely magnetised, only the ion and electron from the annular flux tubes (figure 2) are collected, and the fluxes saturate with the magnetic field increase, as do the floating potential. That saturation indicated that the diffusion parallel to the magnetic field dominates the perpendicular diffusion; in other terms, the influence of the magnetic field is more significant than the collisional effects. At 2 Pa with Ar, this saturation is reached around 135 mT (figure 4). That corresponds to the magnetic field at which $\lambda_i \approx r_{Li}/3$ (figure 4), which corresponds to the commonly taken criteria of plasma magnetisation.

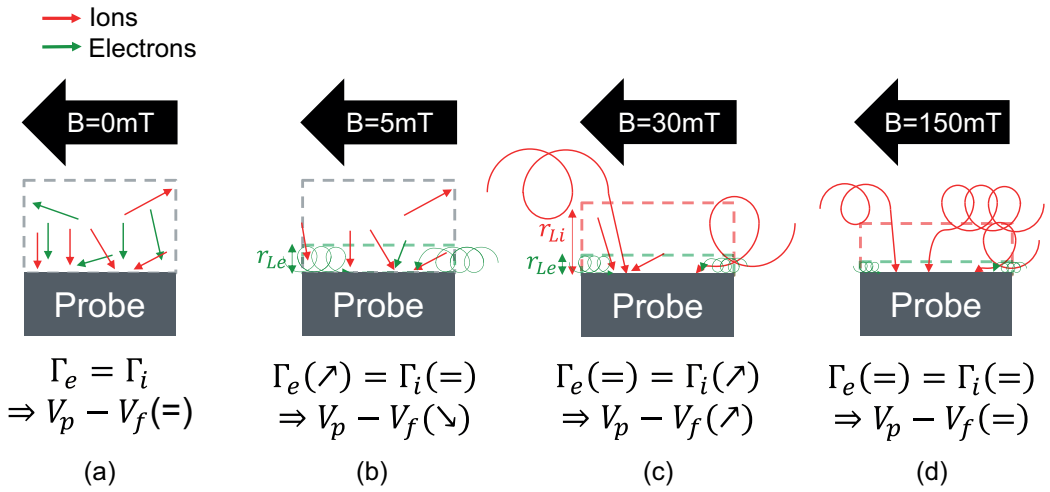

Figure 10: Schematic of ions and electrons collected by the radial probe for different B field magnitudes at 2 Pa. The symbol between the brackets indicates if the fluxes or the potential increase ($\nearrow$), decrease ($\searrow$) or are stable ($=$).

On the contrary, as mentioned previously, the planar probe mainly depends on parallel diffusion. In the case of a floating probe, the planar elec-

trode collects ions from a flux tube of radius $r_{pri} = r_{pr} + r_{Li}$ and electrons from a flux tube with a radius $r_{pre} = r_{pr} + r_{Le}$, where r_{pr} the radius of the planar electrode (figure 2). r_{Li} is comparable to the probe radius at a low B field ($\approx$ 40 mT), and then the planar probe floating potential follows the plasma potential above 60 mT to maintain the zero net current on the probe.

4. Conclusion and outlook

The influence of the magnetic field strength on several plasma parameters (V_{DC}, V_p, V_f, T_e) was measured for different gases and pressures. Additionally, for Ar discharges at 1 Pa, the variation of the density n_e along the perpendicular direction was determined.

The main results are summarised as follows:

- The self-bias saturated with the increase of the magnetic field. This saturation occurred roughly when $r_{Li} \approx \lambda_i$. The variation of the self-bias was associated with the variation of the collection area of charged particles in the plasma. The observed pressure dependence was consistent and enabled collision cross-section calculation in the magnetised discharge. The calculated cross-section matched the literature. Additionally, the planar floating potential and self-bias saturation magnetic threshold trend were compatible with the kinetic theory for the collisional mean free path.

- Two main features were observed in the plasma and floating potential variation. First, the potential in the bulk plasma decreased as the electron collection area decreased. Secondly, when ions started to get magnetised, the radial floating potential increased to reach saturation when the ions were magnetised. The saturation of the floating potential on the radial probe happened when the ion gyroradius was 2 to 3 times smaller than the ion-neutral mean free path, indicating magnetisation of the ions.

- Likewise, plasma excitation frequency did not affect the saturation magnetic threshold.

The experiments presented here provide important results on ion magnetisation. The probe floating potential is a good indicator of ion magnetisation. Additionally, the probe developed in this contribution allows for almost independent measurement of perpendicular and parallel flux.

However, varying the electrode angle to the magnetic field could seriously impact the ions' magnetisation, especially in the sheath, as the perpendicular ion speed increased with the angle. Future experimental works with varying angles are planned regarding the impact of the electrode tilt on the magnetisation in the plasma sheath [39].

5. Acknowledgements

This work has been funded by the Swiss National Science Foundation under agreement No 200021E_189448. This work is supported by the French National Research Agency (ANR) under project SHEAR ANR-19-CE30-033-01. This work was supported by the Swiss State Secretariat for Education, Research and Innovation (SERI) under contract number 22.00424. The authors would like to thank the Swiss Federal Office of Energy, the Swiss Nanoscience Institute and the Federal Office for Education and Science for their Financial support.

References

[1] J.-P. Boeuf, Rotating structures in low temperature magnetized plasmas—insight from particle simulations, Frontiers in Physics 2 (2014). doi:10.3389/fphy.2014.00074.
URL https://www.frontiersin.org/articles/10.3389/fphy.2014.00074

[2] A. Tavant, V. Croes, R. Lucken, T. Lafleur, A. Bourdon, P. Chabert, The effects of secondary electron emission on plasma sheath characteristics and electron transport in an ExB discharge via kinetic simulations, Plasma Sources Science and Technology 27 (12) (2018) 124001, publisher: IOP Publishing. doi:10.1088/1361-6595/aaeccd.
URL https://doi.org/10.1088/1361-6595/aaeccd

[3] N. P. Brown, M. L. R. Walker, Review of Plasma-Induced Hall Thruster Erosion, Applied Sciences 10 (11) (2020) 3775, number: 11 Publisher: Multidisciplinary Digital Publishing Institute. doi:10.3390/app10113775.
URL https://www.mdpi.com/2076-3417/10/11/3775

[4] M. D. Carter, P. M. Ryan, D. Hoffman, W. S. Lee, D. Buchberger, V. Godyak, Combined rf and transport effects in magnetized capacitive discharges, Journal of Applied Physics 100 (7) (2006) 073305, publisher: American Institute of Physics. doi:10.1063/1.2355436.
URL https://aip.scitation.org/doi/full/10.1063/1.2355436

[5] M. A. Lieberman, A. Lichtenberg, Principles of Plasma Discharges and Materials Processing, 2nd Edition, Wiley, New York, NY, USA, 2005.
URL https://onlinelibrary.wiley.com/doi/book/10.1002/0471724254

[6] W. Teh, R. Caramto, S. Arkalgud, T. Saito, K. Maruyama, K. Maekawa, Magnetically-enhanced capacitively-coupled plasma etching for 300 mm wafer-scale fabrication of Cu through-silicon-vias for 3D logic integration, in: 2009 IEEE International Interconnect Technology Conference, 2009, pp. 53–55, iSSN: 2380-6338. doi:10.1109/IITC.2009.5090338.

[7] L. Wang, M. Vass, Z. Donkó, P. Hartmann, A. Derzsi, Y.-H. Song, J. Schulze, Magnetic attenuation of the self-excitation of the plasma series resonance in low-pressure capacitively coupled discharges, Plasma Sources Science and Technology 30 (10) (2021) 10LT01, publisher: IOP Publishing. doi:10.1088/1361-6595/ac287b.
URL https://doi.org/10.1088/1361-6595/ac287b

[8] P. K. Yadav, M. Kumar, S. K. Rai, J. A. Chakera, C. Mukherjee, M. Nayak, P. A. Naik, G. S. Lodha, Cleaning of optical surfaces by capacitively coupled RF discharge plasma, AIP Conference Proceedings 1591 (1) (2014) 890–892, publisher: American Institute of Physics. doi:10.1063/1.4872792.
URL https://aip.scitation.org/doi/abs/10.1063/1.4872792

[9] M. G. Cuxart, J. Reyes-Herrera, I. Šics, A. R. Goñi, H. M. Fernandez, V. Carlino, E. Pellegrin, Remote plasma cleaning of optical surfaces: Cleaning rates of different carbon allotropes as a function of RF powers and distances, Applied Surface Science 362 (2016) 448–458. doi:10.1016/j.apsusc.2015.11.117.
URL https://www.sciencedirect.com/science/article/pii/S0169433215028123

[10] A. Ushakov, A. Verlaan, R. Ebeling, C.-C. Wu, R. O'Neill, M. Smith, B. Stratton, N. Koster, A. Gattuso, C. J. Lasnier, R. Feder, M. P. Maniscalco, P. Verhoeff, UWAVS first mirror after long plasma cleaning: Surface properties and material redeposition issues, Fusion Engineering and Design 146 (2019) 1559–1563. doi:10.1016/j.fusengdes.2019.02.128.
URL https://www.sciencedirect.com/science/article/pii/S0920379619303102

[11] P. Chabert, N. Braithwaite, Physics of Radio-Frequency Plasmas, Cambridge University Press, Cambridge, 2011.

[12] T. V. Tsankov, P. Chabert, U. Czarnetzki, Foundations of magnetized radio-frequency discharges, Plasma Sources Science and Technology (2022). doi:10.1088/1361-6595/ac869a.
URL http://iopscience.iop.org/article/10.1088/1361-6595/ac869a

[13] M. Stanojević, M. Čerček, T. Gyergyek, Experimental Study of Planar Langmuir Probe Characteristics in Electron Current-Carrying Magnetized Plasma, Contributions to Plasma Physics 39 (3) (1999) 197–222, _eprint: https://onlinelibrary.wiley.com/doi/pdf/10.1002/ctpp.2150390303. doi:10.1002/ctpp.2150390303.
URL https://onlinelibrary.wiley.com/doi/abs/10.1002/ctpp.2150390303

[14] V. Demidov, S. Ratynskaia, K. Rypdal, The Analysis of Probe I-V Characteristics in a Magnetized Low-Temperature Plasma, Contributions to Plasma Physics 41 (5) (2001) 443–448. doi:10.1002/1521-3986(200109)41:5<443::AID-CTPP443>3.0.CO;2-K.

[15] J. Ledig, E. Faudot, J. Moritz, S. Heuraux, N. Lemoine, M. Usoltceva, Experimental and theoretical study of bumped characteristics obtained with cylindrical Langmuir probe in magnetized helium plasma, Plasma Sources Science and Technology 29 (3) (2020) 035007, publisher: IOP Publishing. doi:10.1088/1361-6595/ab56d2.
URL https://doi.org/10.1088/1361-6595/ab56d2

[16] S. Dahiya, P. Singh, S. Das, N. Sirse, S. K. Karkari, Magnetic field induced electron temperature inhomogeneity effects on discharge properties in cylindrical capacitively coupled plasmas, Physics Letters A 468 (2023) 128745. doi:10.1016/j.physleta.2023.128745.
URL https://www.sciencedirect.com/science/article/pii/S0375960123001251

[17] S. Yadav, S. Ghosh, S. Bose, K. K. Barada, R. Pal, P. K. Chattopadhyay, Role of ion magnetization in formation of radial density profile in magnetically expanding plasma produced by helicon antenna, Physics of Plasmas 25 (4) (2018) 043518. doi:10.1063/1.5028576.
URL https://doi.org/10.1063/1.5028576

[18] F. Filleul, A. Caldarelli, R. Boswell, C. Charles, N. Rattenbury, J. Cater, The role of ion magnetization on plasma generation in a magnetic nozzle rf device, Journal of Electric Propulsion 1 (1) (2022) 20. doi:10.1007/s44205-022-00021-y.
URL https://doi.org/10.1007/s44205-022-00021-y

[19] V. A. Ryabyi, V. A. Obukhov, On the reliability of probe diagnostics in RF plasma, Plasma Physics Reports 39 (13) (2013) 1130–1135. doi:10.1134/S1063780X13050164.
URL https://doi.org/10.1134/S1063780X13050164

[20] F. F. Chen, Introduction to Plasma Physics and Controlled Fusion, Springer International Publishing, Cham, 2016. doi:10.1007/978-3-319-22309-4.
URL http://link.springer.com/10.1007/978-3-319-22309-4

[21] M. Stanojević, M. Čerček, T. Gyergyek, N. Jelić, Interpretation of a Planar Langmuir Probe Current — Voltage Characteristic in a Strong Magnetic Field, Contributions to Plasma Physics 34 (5) (1994) 607–633. doi:10.1002/ctpp.2150340502.

[22] M. Stanojević, M. Čerček, T. Gyergyek, N. Jelić, Diffusion Model of Saturation Current Collection by a Planar Langmuir Probe in a Strong Magnetic Field, Contributions to Plasma Physics 33 (4) (1993) 241–264, _eprint: https://onlinelibrary.wiley.com/doi/pdf/10.1002/ctpp.2150330402. doi:10.1002/ctpp.2150330402.

URL https://onlinelibrary.wiley.com/doi/abs/10.1002/ctpp.2150330402

[23] K. Köhler, D. E. Horne, J. W. Coburn, Frequency dependence of ion bombardment of grounded surfaces in rf argon glow discharges in a planar system, Journal of Applied Physics 58 (9) (1985) 3350–3355, publisher: American Institute of Physics. doi:10.1063/1.335797.
URL https://aip.scitation.org/doi/10.1063/1.335797

[24] P. Hiret, P. Tognina, E. Faudot, R. Steiner, A. Dmitriev, L. Marot, E. Meyer, Variations of plasma potential in RF discharges with DC-grounded electrode, Plasma Sources Science and Technology 33 (7) (2024) 075019, publisher: IOP Publishing. doi:10.1088/1361-6595/ad6691.
URL https://dx.doi.org/10.1088/1361-6595/ad6691

[25] A. Caldarelli, Radio-Frequency Plasma Expansion in Different Magnetic Nozzle Configurations, Thesis, ResearchSpace@Auckland, accepted: 2024-03-25T20:32:26Z (2024).
URL https://researchspace.auckland.ac.nz/handle/2292/67855

[26] P. Hiret, K. Soni, A. C. Mana, E. Faudot, L. Moser, R. Steiner, A. Geraldini, S. Alberti, I. Furno, J. Moritz, F. Brochard, S. Heuraux, L. Marot, E. Meyer, Plasma sputtering of biased electrodes in an oblique magnetic field, Plasma Sources Science and Technology 32 (9) (2023) 095021, publisher: IOP Publishing. doi:10.1088/1361-6595/acfc63.
URL https://dx.doi.org/10.1088/1361-6595/acfc63

[27] G. A. Hebner, A. M. Paterson, Ion temperature and velocity in a 300 mm diameter capacitively coupled plasma reactor driven at 13, 60 and 162 MHz, Plasma Sources Science and Technology 19 (1) (2010) 015020. doi:10.1088/0963-0252/19/1/015020.
URL https://dx.doi.org/10.1088/0963-0252/19/1/015020

[28] H.-J. Woo, K.-S. Chung, M.-J. Lee, T. Lho, The effects of plasma density and magnetic field on ion temperature and drift velocity in a LaB6 direct current plasma, Physics of Plasmas 16 (2) (2009) 023505. doi:10.1063/1.3076205.
URL https://doi.org/10.1063/1.3076205

[29] J. Ledig, E. Faudot, J. Moritz, S. Heuraux, N. Lemoine, S. Devaux, Experimental and theoretical study of density, potential, and current structures of a helium plasma in front of an radio frequency antenna tilted with respect to the magnetic field lines, Contributions to Plasma Physics 60 (10) (2020) e202000072, _eprint: https://onlinelibrary.wiley.com/doi/pdf/10.1002/ctpp.202000072. doi:10.1002/ctpp.202000072.
URL https://onlinelibrary.wiley.com/doi/abs/10.1002/ctpp.202000072

[30] S. A. Khrapak, Practical expression for an effective ion-neutral collision frequency in flowing plasmas of some noble gases, Journal of Plasma Physics 79 (6) (2013) 1123–1124. doi:10.1017/S0022377813001025.
URL https://www.cambridge.org/core/product/identifier/S0022377813001025/type/journal_article

[31] S. Imazu, Collision frequency of charged particles in a weekly ionized gas in a strong magnetic field, Physical Review A 23 (5) (1981) 2644–2649, publisher: American Physical Society. doi:10.1103/PhysRevA.23.2644.
URL https://link.aps.org/doi/10.1103/PhysRevA.23.2644

[32] A. V. Phelps, The application of scattering cross sections to ion flux models in discharge sheaths, Journal of Applied Physics 76 (2) (1994) 747–753. doi:10.1063/1.357820.
URL https://doi.org/10.1063/1.357820

[33] S. A. Maiorov, Ion drift in a gas in an external electric field, Plasma Physics Reports 35 (9) (2009) 802–812. doi:10.1134/S1063780X09090098.
URL http://link.springer.com/10.1134/S1063780X09090098

[34] D. Benyoucef, M. Yousfi, B. Belmadani, A. Settaouti, PIC MC Using Free Path for the Simulation of Low-Pressure RF Discharge in Argon, IEEE Transactions on Plasma Science 38 (4) (2010) 902–908. doi:10.1109/TPS.2010.2042305.
URL http://ieeexplore.ieee.org/document/5433004/

[35] J. C. Maxwell, V. Illustrations of the dynamical theory of gases.—Part I. On the motions and collisions of perfectly elastic spheres, The

London, Edinburgh, and Dublin Philosophical Magazine and Journal of Science 19 (124) (1860) 19–32, publisher: Taylor & Francis _eprint: https://doi.org/10.1080/14786446008642818. doi:10.1080/14786446008642818.
URL https://doi.org/10.1080/14786446008642818

[36] J. W. Coburn, E. Kay, Positive-ion bombardment of substrates in rf diode glow discharge sputtering, Journal of Applied Physics 43 (12) (1972) 4965–4971, publisher: American Institute of Physics. doi:10.1063/1.1661054.
URL https://aip.scitation.org/doi/abs/10.1063/1.1661054

[37] F. Filleul, A. Caldarelli, K. Takahashi, R. W. Boswell, C. Charles, J. E. Cater, N. Rattenbury, Helicon waves in a converging-diverging magnetoplasma, Plasma Sources Science and Technology 32 (11) (2023) 115015, publisher: IOP Publishing. doi:10.1088/1361-6595/ad0b96.
URL https://dx.doi.org/10.1088/1361-6595/ad0b96

[38] K. Soni, S. Iyyakkunnel, R. Steiner, R. Antunes, L. Moser, O. Bieri, L. Marot, E. Meyer, Effect of 3T magnetic field on RF plasma sputtering in a ITER-relevant first mirror unit, Nuclear Fusion (2022). doi:10.1088/1741-4326/ac8b20.
URL http://iopscience.iop.org/article/10.1088/1741-4326/ac8b20

[39] P. Hiret, J. Moritz, A. Dmitriev, R. Steiner, E. Faudot, F. Brochard, S. Heuraux, E. Meyer, Investigation of the sheath potential profile in magnetised RF plasma using a floating probe, Under preparation.